Supplement of

Larger than expected organic acid yields from the multi-generation oxidation of petrochemical alkenes

Baocong Zhao[1,2], Luxin Ren[1,2], Sihao Lin[1,2], Yongpeng Ji[1,2], Jiaxin Wang[1,2], Tao Ma[1,2], Yuemeng Ji[*,1,2], Taicheng An[1,2]

[1] Guangdong-Hong Kong-Macao Joint Laboratory for Contaminants Exposure and Health, Guangdong Key Laboratory of Environmental Catalysis and Health Risk Control, Institute of Environmental Health and Pollution Control, Guangdong University of Technology, Guangzhou 510006, China
[2] Guangzhou Key Laboratory of Environmental Catalysis and Pollution Control, Key Laboratory for City Cluster Environmental Safety and Green Development of the Ministry of Education, School of Environmental Science and Engineering, Guangdong University of Technology, Guangzhou 510006, China

Correspondence to: Prof. Yuemeng Ji (jiym@gdut.edu.cn)

The copyright of individual parts of the supplement might differ from the article license.

This PDF file includes:

Supplementary text

Figures S1 to S10

Tables S1 to S14

References

S1 Search and calculation of multi-conformers

For the H-shift reactions of RO_2 radicals, reactants, transition states, and products have multiple conformers. Previous studies have demonstrated that the reaction kinetics of multi-conformer involvement are more precise than that of single-conformer approximation. Herein, the multi-conformer treatment is performed to investigate the H-shift reactions of RO_2 radicals. A conformer search within the Molclus program is employed to generate a pool of conformers for RO_2 radicals. The selected conformers are further optimized at the M06-2X/6-311+G(2df,2p) level of theory, followed by single-point energy calculations at the DLPNO-CCSD(T)/aug-cc-pVTZ level of theory. On the basis of the calculated reaction energies, the Boltzmann populations (w_i) of each RO_2 conformer are expressed as Eq. (1):

$$w_i = \frac{e^{-\Delta E_i / k_b T}}{\sum_i e^{-\Delta E_i / k_b T}} \quad (1)$$

where ΔE_i is the relative electronic energy barrier of conformer i, k_b is Boltzmann's constant, and T is temperature in Kelvin.

S2 Kinetics calculations

For the BU + OH reactions with pre-reactant complexes, the rate constants are calculated as follows:

$$\mathrm{BU + OH} \overset{K_{eq}}{\leftrightarrow} \mathrm{IM} \overset{k_0}{\rightarrow} \mathrm{P} \quad (2)$$

$$k_1 = K_{eq}\, k_0 \quad (3)$$

where K_{eq} and k_0 are the equilibrium constant for the process of pre-reactant complex formation and the rate constant for the unimolecular reaction of pre-reactant complex, respectively. k_1 is the total rate constant for the BU + OH reactions.

For the unimolecular reactions, especially for the H-shift reactions of peroxy radicals, the rate constants were determined by employing the multi-conformer transition state theory (MC-TST) approach (Møller et al., 2016). The MC-TST rate constant ($k_{MC\text{-}TST}$) was calculated by the sum of individual intrinsic reaction coordinate TST (IRC-TST) rate constants $k_{IRC\text{-}TST}$, each weighted by the Boltzmann population of the corresponding reactant conformers, as shown in Eq. (4) (Chen et al., 2022):

$$k_{\text{MC-TST}} = \sum_{i}^{\text{all TS conf.}} w_i \times k_{\text{IRC-TST}i} \quad (4)$$

where $k_{\text{IRC-TST}i}$ represents the rate constant of conformer i, and w_i is the relative Boltzmann population of the corresponding reactant connected to TS_i.

S3. Kinetic modelling of CH_3COOH formation

Kinetic modelling using calculated rate constants is carried out using the AtChem 2 Program (Sommariva et al., 2020) to estimate the formation rates and yields of CH_3COOH. We include all oxidation initiation pathways and the subsequent steps of the studied *cis*-BU and *trans*-BU in the simulation.

In the simulation, initial concentration of BU, NO, and NO_2 are set to 5 ppb (1.23×10^{11} molecule cm^{-3}), 2 ppb (4.92×10^{10} molecule cm^{-3}), and 17 ppb (4.18×10^{11} molecule cm^{-3}), respectively. These concentrations are the average concentration in the petrochemical regions (Yang et al., 2023; Yang et al., 2024). Besides, the effects of [OH] and [NO] on the oxidation of BU to yield CH_3COOH were tested using variable concentrations of OH (8×10^5 – 1×10^7 molecule^{-1} cm^{-3}) and variable concentrations of NO (0.1 – 20 ppb, i.e., 2.46×10^{10} – 5.00×10^{10} molecule cm^{-3}).

S4. Observation-based chemical box model simulation

The Observation-Based Model for estimating organic acids formation by photochemistry of volatile organic compounds (VOCs), which was built on the MCM v3.3.1 mechanism (Jenkin et al., 1997; Saunders et al., 2003). In this study, we used the field data on VOCs, O_3, NO, NO_2, SO_2, CO and physical values to constrain the boundary of the model and input them into the model for calculation. The photolysis frequency data were calculated from the Tropospheric Ultraviolet and Visible (TUV v5.3.1) model. According to the previous field measurements, in a petrochemical industrial city, alkanes, alkenes, halocarbons, and aromatics contribute 45.3%, 24.0%, 16.5%, and 10.0% respectively to the total volatile organic compounds (TVOCs) (Yang et al., 2024). To simplify the simulation process, this study selects propane, *cis*-2-butene, toluene, and *cis*-1,2-dichloroethylene as representative species for alkanes, alkenes, aromatics, and halocarbons in regional emissions of VOCs. The initial simulated concentrations of these four substances are detailed in Table S13. Furthermore,

constraining the [OH] value according to field data brings the model simulation results closer to the actual atmospheric oxidative capacity. Before the simulation, the model commences at 00:00 LT and is pre-run for 4 days under constraints of the input data which could make unmeasured species reach a steady condition in the sampling field. For the CH_3COOH formation rate ($P(CH_3COOH)$) is listed as follows:

$$P(CH_3COOH) = k_{BU+O3}[O_3] + k_{BU+OH}[OH] \quad (5)$$

here, k refers to the corresponding reaction constant.

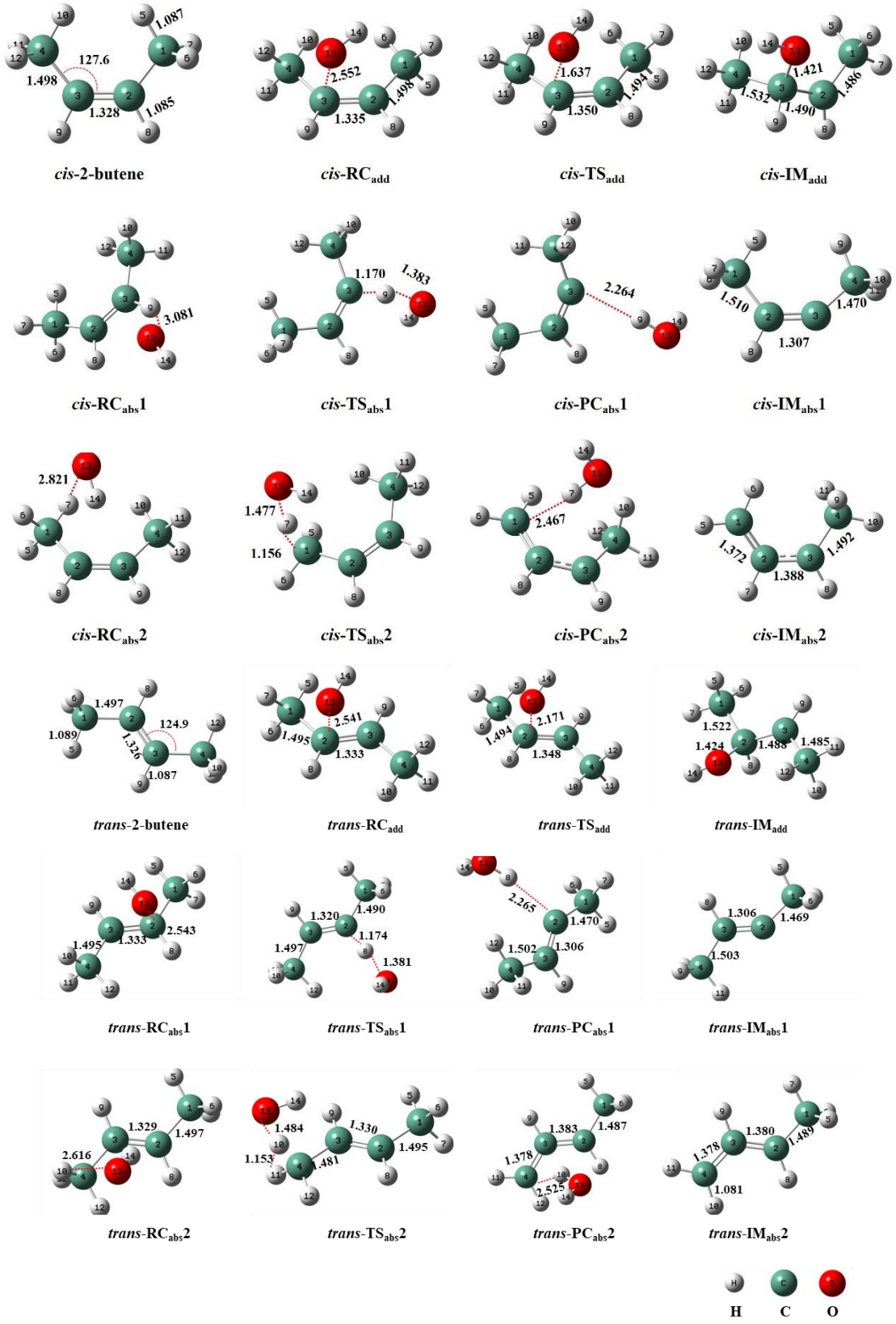

Figure S1. Geometries of all stationary points for initial reaction of *cis*-BU and *trans*-BU with OH optimized at the M06-2X/6-311+G(2df,2p) level of theory.

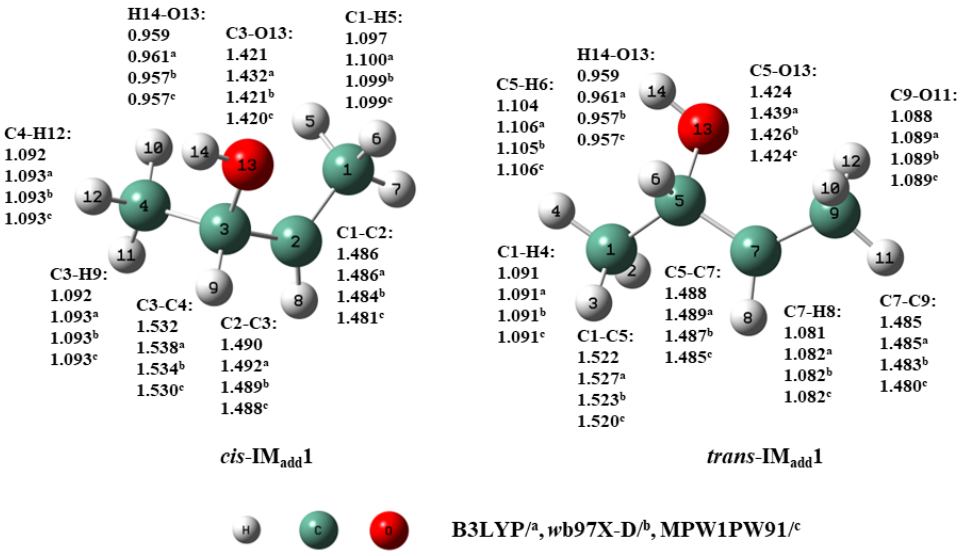

Figure S2. The comparison of the geometries of *cis*-BU and *trans*-BU calculated at the M06-2X/6-311+G(2df,2p) level of theory and other levels (angle in °, bond in Å). [a]B3LYP/6-311+G(2df,2p), [b]MPW1PW91/6-311+G(2df,2p), and ωB97X-D/6-311+G(2df,2p) levels of theory.

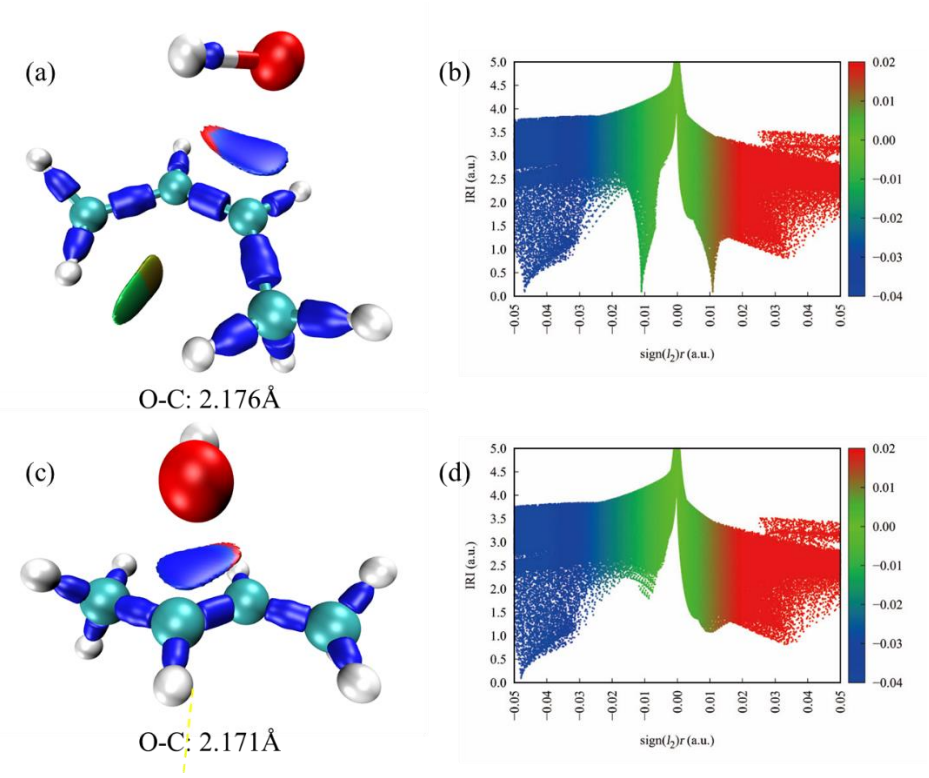

Figure S3. The interaction region indicator (IRI) analyses for (a) *cis*-$TS_{add}1$ and (c) *trans*-$TS_{add}1$, (b) and (d) are the corresponding IRI vs. sign(*l*2)*r* scatterplots. Red, green and blue colors correspond to chemical bonding, van der Waals and site barrier interactions, respectively.

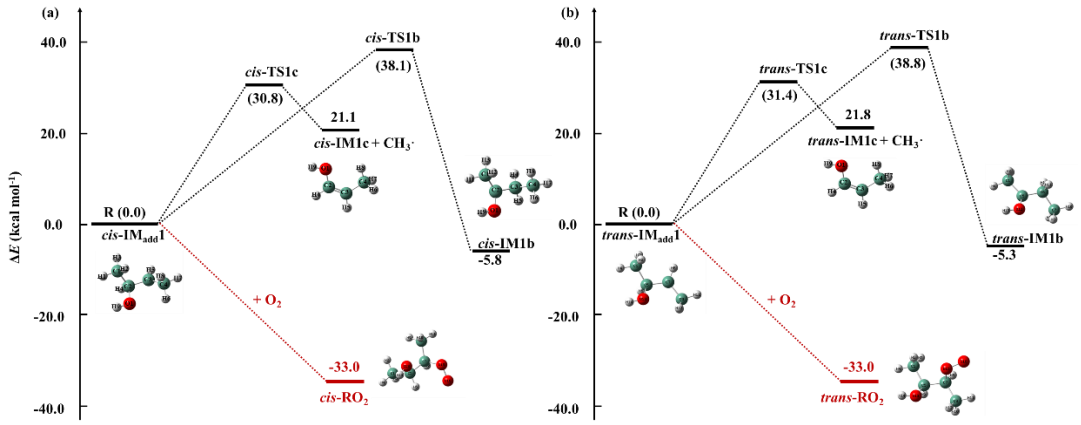

Figure S4. PES for the reaction of (a) *cis*-$IM_{add}1$ and (b) *trans*-$IM_{add}1$ predicted at the DLPNO-CCSD(T)/aug-cc-pVTZ//M06-2X/6-311+G(2df,2p) level of theory (in kcal mol^{-1}).

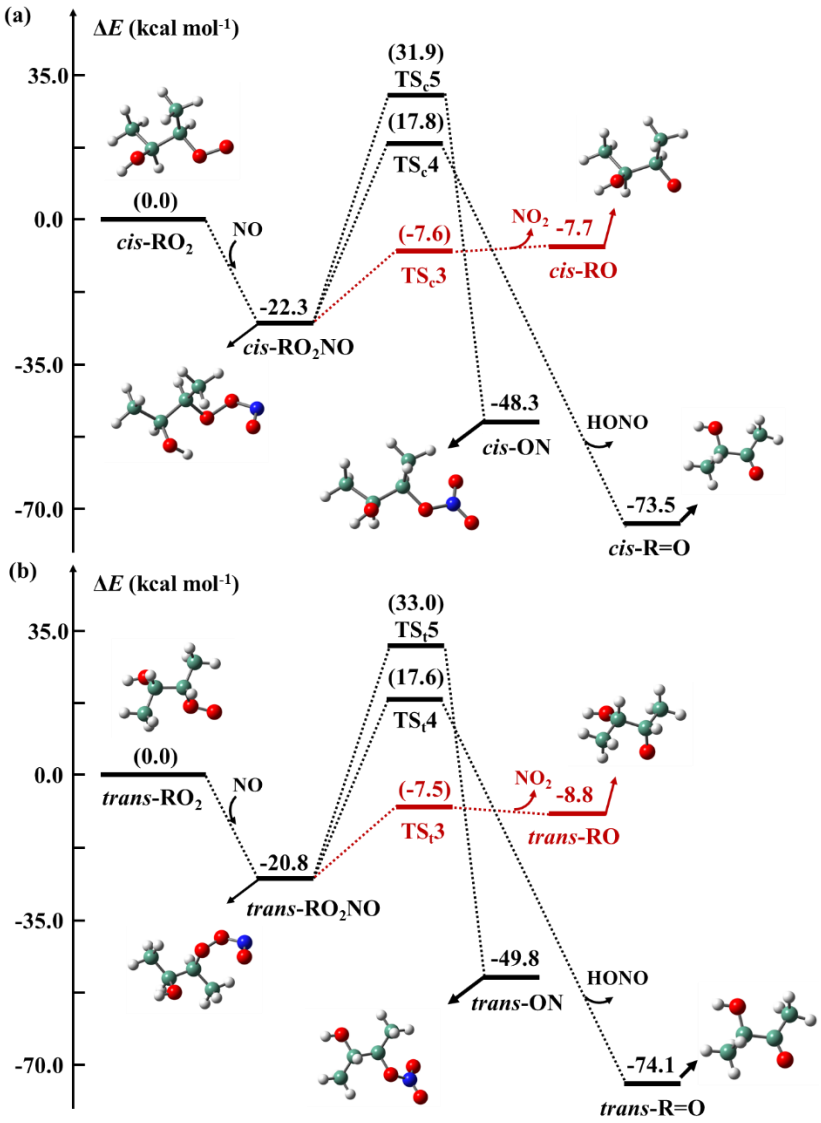

Figure S5. PESs for the reaction systems of (a) *cis*-IM3 + NO and (b) *trans*-IM3 + NO (in kcal mol^{-1}). The red line indicates the dominant pathway.

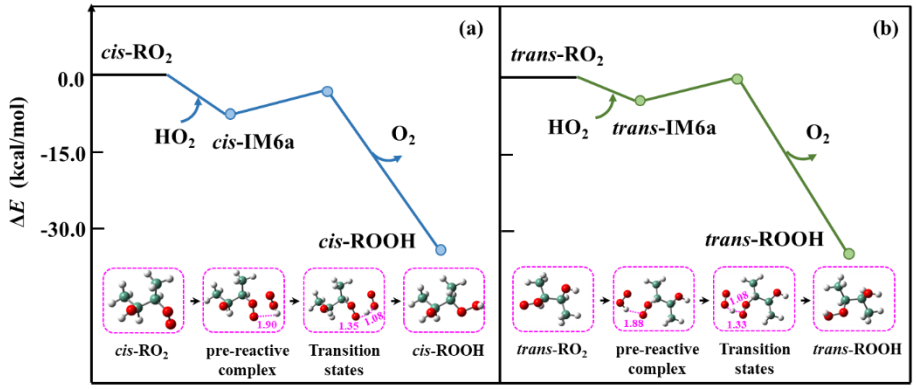

Figure S6. PESs for the (a) *cis*-RO_2 + HO_2 and (b) *trans*-RO_2 + HO_2 reactions predicted at the DLPNO-CCSD(T)/aug-cc-pVTZ//M06-2X/6-311+G(2df,2p) level of theory (in kcal mol^{-1}).

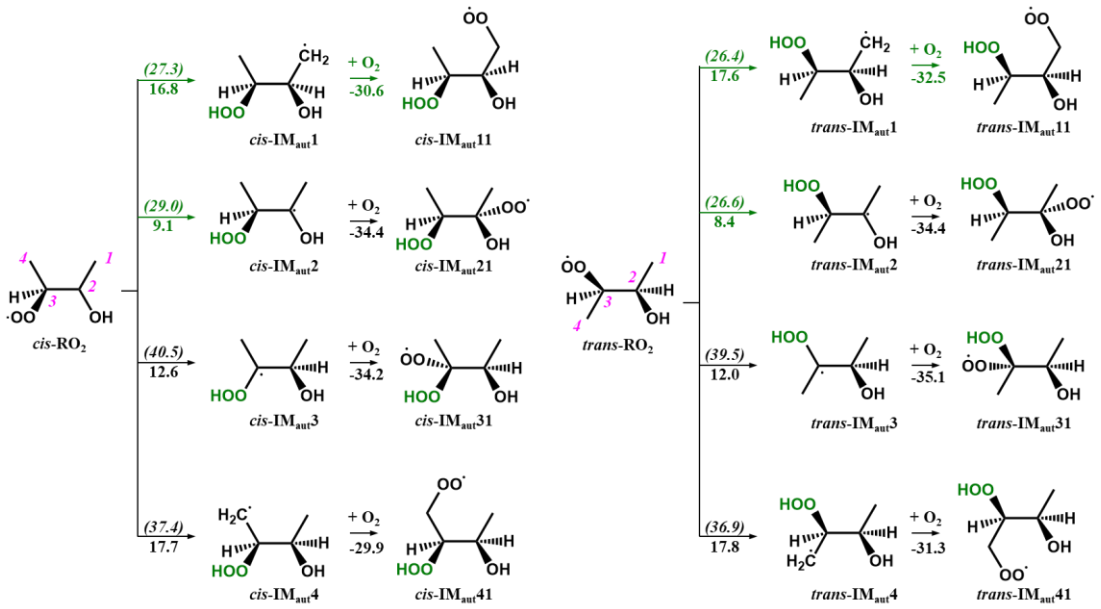

Figure S7. The auto-oxidation reaction mechanism of *cis*-IM3 and *trans*-IM3, with the energy barriers $\Delta E_a^{\#}$ (italic within parentheses, kcal mol^{-1}) and reaction energies ΔE_r (kcal mol^{-1}) predicted at the DLPNO-CCSD(T)/aug-cc-pVTZ//M06-2X/6-311+G(2df,2p) level of theory.

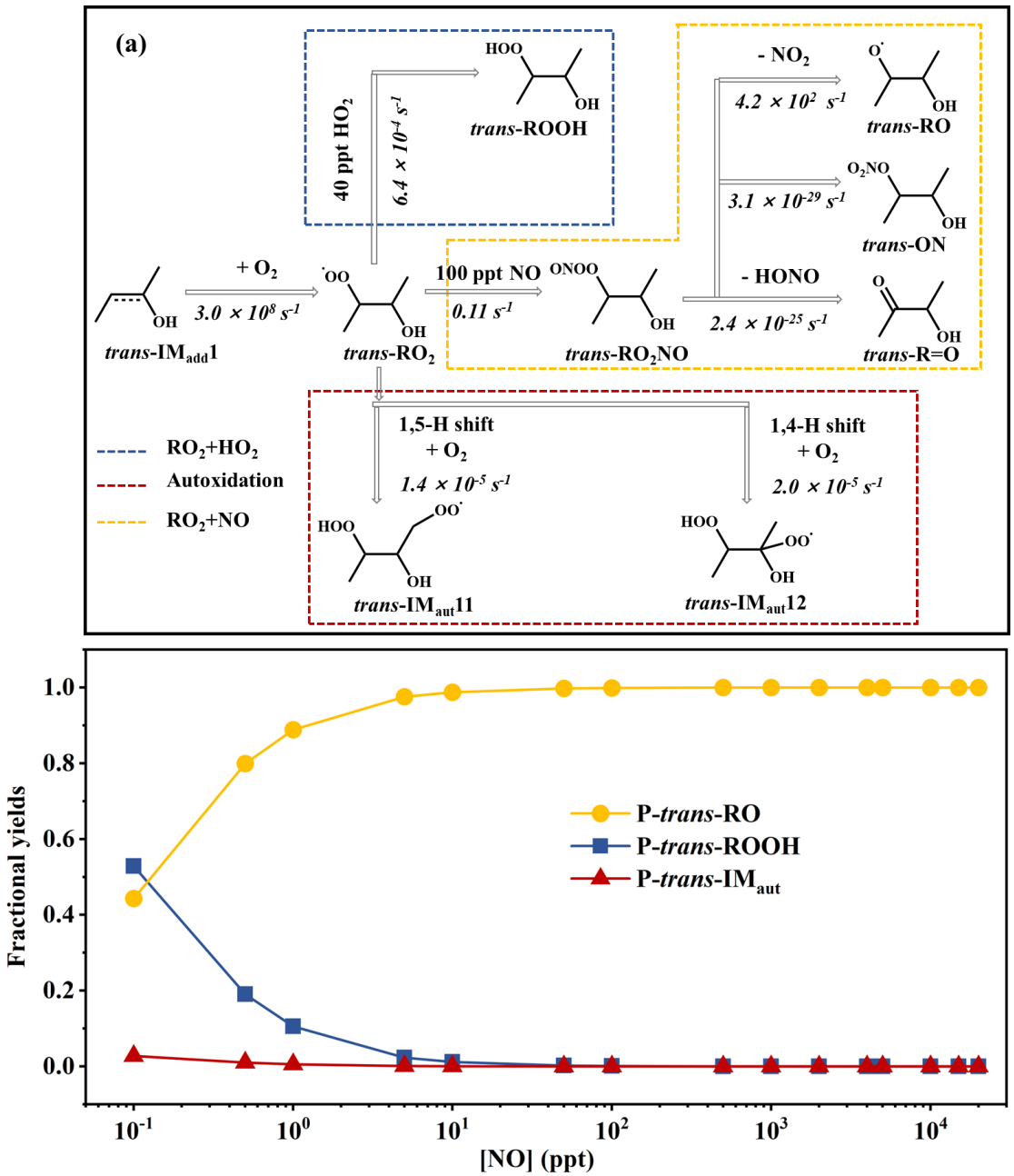

Figure S8. (a) Main reaction pathways for the atmospheric oxidation of *trans*-$IM_{add}1$, under the conditions of 100 ppt NO and 40 ppt HO_2. The reaction rate constants (in s^{-1}) for the crucial reaction pathways are presented in black italic numbers. (b) Simulated fractional yields of transformation products for the atmospheric reactions of *trans*-$IM_{add}1$ as functions of [NO] at 298 K.

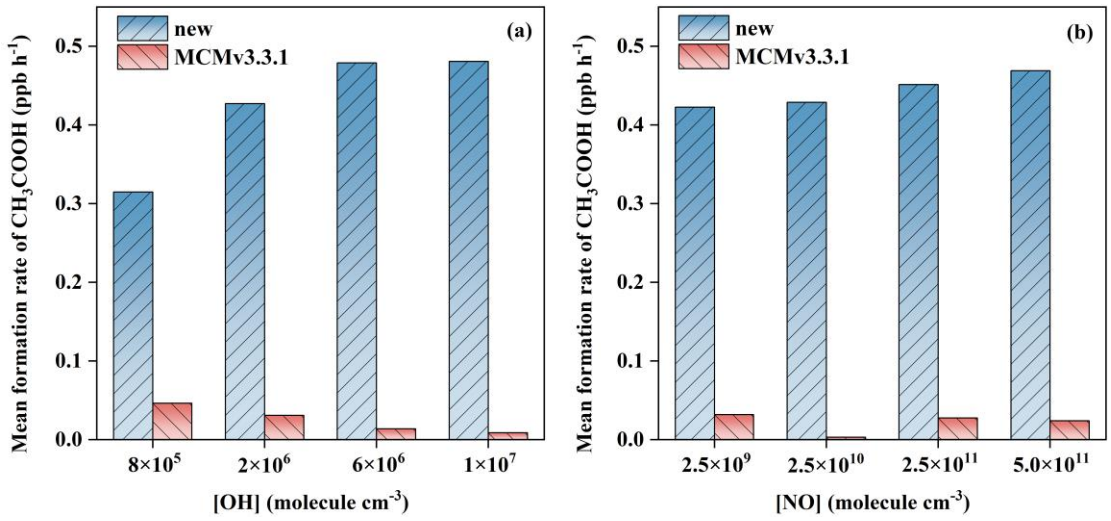

Figure S9. Mean formation rate of CH_3COOH (unit: ppb h^{-1}) from the *trans*-BU + OH reactions as a function of (a) OH concentration ([OH]) and (b) NO concentration ([NO]) under the petrochemical region conditions. The comparison is made between the MCM v3.3.1 and the new mechanism.

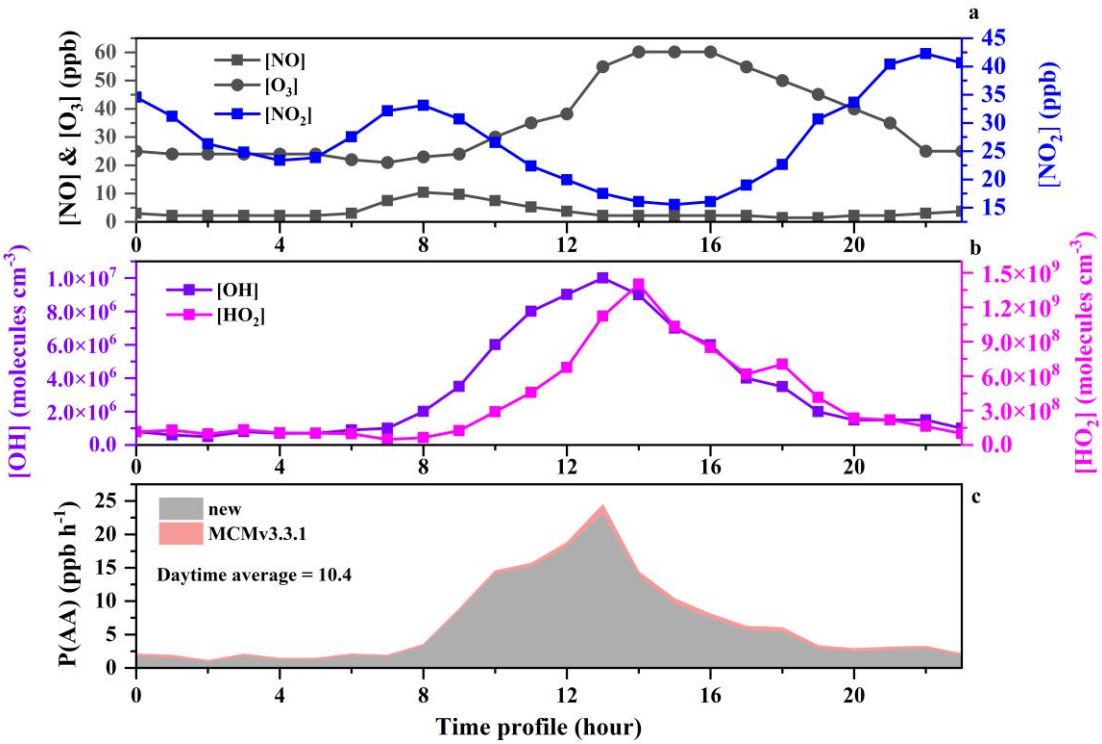

Figure S10. (a-b) Diurnal variations of NO, NO_2, O_3, OH and HO_2 in the petrochemical regions. (c) Simulated daytime (06:00-18:00 LT) formation rate of CH_3COOH.

Table S1. The bond dissociation energies (D^0_{298}(C-H) of different C-H bonds for the *cis*-BU + OH and the *trans*-BU + OH reactions predicted at the DLPNO-CCSD(T)/aug-cc-pVTZ//M06-2X/6-311+G(2df,2p) level of theory.

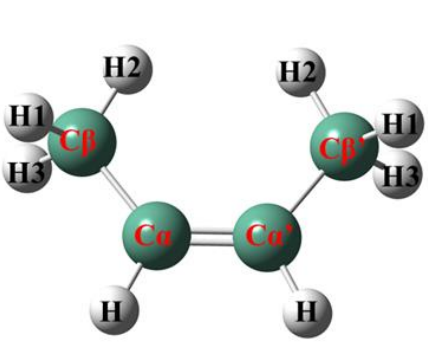

***cis*-BU**

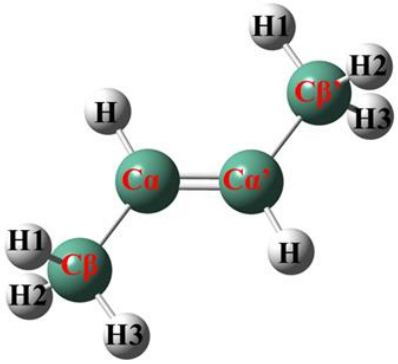

***trans*-BU**

Compounds	Bond	D^0_{298}(C-H (kcal mol^{-1})
cis-BU	Cα-H	98.40
	Cβ-H1	79.72
trans-BU	Cα-H	98.36
	Cβ-H1	78.28

Table S2. The relative energies (ΔE) for pre-reactive complexes and barrier heights ($\Delta E_a^{\#}$) for the initial reactions of BUs with OH radical (kcal mol^{-1}).

Reaction	ΔE	$\Delta E_a^{\#}$
cis-$R_{add}1$	-1.6[a], -1.1[b]	-1.6[a], -1.0[b]
cis-$R_{abs}1$	-2.0[a], -1.5[b]	3.3[a], 3.8[b]
cis-$R_{abs}2$	-2.3[a], -1.8[b]	1.8[a], 2.4[b]
trans-$R_{add}1$	-1.9[a], -1.4[b]	-2.0[a], -1.3[b]
trans-$R_{abs}1$	-2.0[a], -1.4[b]	3.3[a], 3.8[b]
trans-$R_{abs}2$	-2.4[a], -2.0[b]	1.8[a], 2.3[b]

a and b represent without and with considering the BSSE correction.

Table S3. *L* parameter of forming O-H bond and breaking C-H bond in H-abstraction reactions of *cis*-BU and *trans*-BU ($B_R^{(C-H)}$, $B_{TS}^{(C-H)}$, $B_{TS}^{(O-H)}$ and $B_P^{(O-H)}$ are bond lengths in reactants, TS and products, in unit of Å).

Reaction pathways	Breaking C-H bonds			Forming O-H bond			L_{C-H}/L_{O-H}
	$B_R^{(C-H)}$	$B_{TS}^{(C-H)}$	L_{C-H}	$B_{TS}^{(O-H)}$	$B_P^{(O-H)}$	L_{O-H}	
cis-$R_{abs}1$	1.09	1.17	0.08	1.38	0.96	0.42	0.19
cis-$R_{abs}2$	1.09	1.16	0.07	1.48	0.96	0.52	0.13
trans-$R_{abs}1$	1.09	1.17	0.08	1.38	0.96	0.42	0.19
trans-$R_{abs}2$	1.09	1.15	0.06	1.48	0.96	0.52	0.12

Table S4. Rate constants (cm^3 $molecule^{-1}$ s^{-1}) and branching ratios (%) for the initial reaction of *cis*-BU with the OH radical computed over the temperature range from 240-340 K at 1 atm.

T/K	*cis*-$R_{add}1$		*cis*-$R_{abs}1$		*cis*-$R_{abs}2$		overall rate
	k	Γ	*k*	Γ	*k*	Γ	constants
240	8.90×10^{-11}	99.8%	2.79×10^{-15}	0%	1.52×10^{-13}	0.2%	8.90×10^{-11}
250	7.37×10^{-11}	99.8%	3.55×10^{-15}	0%	1.69×10^{-13}	0.2%	7.37×10^{-11}
260	6.27×10^{-11}	99.7%	4.45×10^{-15}	0%	1.87×10^{-13}	0.3%	6.27×10^{-11}
273	5.15×10^{-11}	99.6%	5.89×10^{-15}	0%	2.12×10^{-13}	0.4%	5.15×10^{-11}
280	4.66×10^{-11}	99.5%	6.79×10^{-15}	0%	2.27×10^{-13}	0.5%	4.66×10^{-11}
290	4.13×10^{-11}	99.4%	8.25×10^{-15}	0%	2.49×10^{-13}	0.6%	4.13×10^{-11}
298	3.74×10^{-11}	99.3%	9.59×10^{-15}	0%	2.67×10^{-13}	0.7%	3.74×10^{-11}
300	3.66×10^{-11}	99.2%	9.94×10^{-15}	0%	2.72×10^{-13}	0.7%	3.66×10^{-11}
310	3.31×10^{-11}	99.1%	1.19×10^{-14}	0%	2.97×10^{-13}	0.9%	3.31×10^{-11}
320	3.02×10^{-11}	98.9%	1.41×10^{-14}	0%	3.23×10^{-13}	1.1%	3.02×10^{-11}
330	2.77×10^{-11}	98.7%	1.66×10^{-14}	0.1%	3.50×10^{-13}	1.3%	2.77×10^{-11}
340	2.54×10^{-11}	98.4%	1.94×10^{-14}	0.1%	3.79×10^{-13}	1.5%	2.54×10^{-11}

Table S5. Rate constants (cm^3 $molecule^{-1}$ s^{-1}) and branching ratios (%) for the initial reaction of *trans*-BU with OH radical computed over the temperature range from 240-340 K at 1 atm.

T/K	*trans*-$R_{add}1$		*trans*-$R_{abs}1$		*trans*-$R_{abs}2$		overall rate
	k	Γ	*k*	Γ	*k*	Γ	constants
240	1.68×10^{-10}	99.8%	3.00×10^{-15}	0%	2.76×10^{-13}	0.2%	1.68×10^{-10}
250	1.34×10^{-10}	99.8%	3.80×10^{-15}	0%	3.11×10^{-13}	0.2%	1.34×10^{-10}
260	1.09×10^{-10}	99.7%	4.75×10^{-15}	0%	3.50×10^{-13}	0.3%	1.09×10^{-10}
273	8.53×10^{-11}	99.5%	6.24×10^{-15}	0%	4.03×10^{-13}	0.5%	8.57×10^{-11}
280	7.61×10^{-11}	99.4%	7.17×10^{-15}	0%	4.35×10^{-13}	0.6%	7.66×10^{-11}
290	6.55×10^{-11}	99.3%	8.69×10^{-15}	0%	4.82×10^{-13}	0.7%	6.59×10^{-11}
298	5.80×10^{-11}	99.1%	1.01×10^{-14}	0%	5.22×10^{-13}	0.9%	5.85×10^{-11}
300	5.64×10^{-11}	99.0%	1.04×10^{-14}	0%	5.32×10^{-13}	0.9%	5.70×10^{-11}
310	4.97×10^{-11}	98.8%	1.24×10^{-14}	0%	5.86×10^{-13}	1.2%	5.03×10^{-11}
320	4.37×10^{-11}	98.5%	1.47×10^{-14}	0%	6.42×10^{-13}	1.4%	4.44×10^{-11}
330	3.92×10^{-11}	98.2%	1.72×10^{-14}	0%	7.03×10^{-13}	1.8%	4.00×10^{-11}
340	3.55×10^{-11}	97.8%	2.01×10^{-14}	0%	7.66×10^{-13}	2.1%	3.63×10^{-11}

Table S6. Rate constants for the reaction with O_2 (R3), isomerization (R4), and decomposition (R5) of *cis*-$IM_{add}1$ and *trans*-$IM_{add}1$ computed in the temperature range from 298 K at 1 atm.

T/*K*	*k*
R3	6.20×10^{-11} cm^3 $molecule^{-1}$ s^{-1}
R4	7.25×10^{-13} s^{-1}
R5	2.62×10^{-10} s^{-1}

Table S7. Rate constants of *cis*-/*trans*-IM3 + NO reactions computed at 240-340 K. s^{-1} for the unimolecular reaction rate constant and cm^3 $molecule^{-1}$ s^{-1} for the bimolecular reaction rate constant.

T/*K*	*k*(*cis*-R6)	*k*(*cis*-R10)	*k*(*cis*-R11)	*k*(*cis*-R12)
240	3.98×10^{-11}	0.19	6.89×10^{-40}	4.35×10^{-37}
250	4.06×10^{-11}	0.65	9.58×10^{-38}	4.55×10^{-35}
260	4.14×10^{-11}	1.99	9.14×10^{-36}	3.35×10^{-33}
273	4.24×10^{-11}	7.51	2.08×10^{-33}	5.59×10^{-31}
280	4.29×10^{-11}	1.46×10^{1}	3.15×10^{-32}	7.24×10^{-30}
290	4.37×10^{-11}	3.58×10^{1}	1.22×10^{-30}	2.27×10^{-28}
298	4.43×10^{-11}	7.01×10^{1}	1.90×10^{-29}	3.03×10^{-27}
300	4.44×10^{-11}	8.25×10^{1}	3.68×10^{-29}	5.67×10^{-27}
310	4.52×10^{-11}	1.80×10^{2}	8.96×10^{-28}	1.15×10^{-25}
320	4.59×10^{-11}	3.76×10^{2}	1.79×10^{-26}	1.94×10^{-24}
330	4.66×10^{-11}	7.49×10^{2}	2.98×10^{-25}	2.76×10^{-23}
340	4.73×10^{-11}	1.43×10^{3}	4.21×10^{-24}	3.37×10^{-22}

T/K	*k*(*trans*-R6)	*k*(*trans*-R10)	*k*(*trans*-R11)	*k*(*trans*-R12)
240	3.98×10^{-11}	1.88	1.24×10^{-39}	1.02×10^{-34}
250	4.06×10^{-11}	5.71	1.69×10^{-37}	8.54×10^{-33}
260	4.14×10^{-11}	1.59×10^{1}	1.58×10^{-35}	5.10×10^{-31}
273	4.24×10^{-11}	5.42×10^{1}	3.50×10^{-33}	6.65×10^{-29}
280	4.29×10^{-11}	9.98×10^{1}	5.23×10^{-32}	7.61×10^{-28}
290	4.37×10^{-11}	2.27×10^{2}	1.99×10^{-30}	2.02×10^{-26}
298	4.43×10^{-11}	4.22×10^{2}	3.06×10^{-29}	2.38×10^{-25}
300	4.44×10^{-11}	4.90×10^{2}	5.92×10^{-29}	4.32×10^{-25}
310	4.52×10^{-11}	1.01×10^{3}	1.42×10^{-27}	7.59×10^{-24}
320	4.59×10^{-11}	1.97×10^{3}	2.80×10^{-26}	1.12×10^{-22}
330	4.66×10^{-11}	3.72×10^{3}	4.61×10^{-25}	1.40×10^{-21}
340	4.73×10^{-11}	6.76×10^{3}	6.45×10^{-24}	1.51×10^{-20}

Table S8. Rate constants (cm^3 $molecule^{-1}$ s^{-1}) of the *cis*-IM3 + HO_2 and *trans*-IM3 + HO_2 reactions computed at 240-340 K.

T/K	*k*(*cis*-R7)	*k*(*trans*-R7)
240	1.71×10^{-11}	2.54×10^{-12}
250	1.14×10^{-11}	1.88×10^{-12}
260	7.96×10^{-12}	1.43×10^{-12}
273	5.23×10^{-12}	1.05×10^{-12}
280	4.25×10^{-12}	9.07×10^{-13}
290	3.24×10^{-12}	7.46×10^{-13}
298	2.65×10^{-12}	6.47×10^{-13}
300	2.53×10^{-12}	6.26×10^{-13}
310	2.01×10^{-12}	5.33×10^{-13}
320	1.63×10^{-12}	4.61×10^{-13}
330	1.35×10^{-12}	4.04×10^{-13}
340	1.12×10^{-12}	3.58×10^{-13}

Table S9. Rate constants (s^{-1}) of the H-shift reactions for *cis*-IM3 and *trans*-IM3 computed at different temperatures.

T/K	*cis*-R8	*cis*-R8b	*cis*-R8c	*cis*-R8d	$k_{MC\text{-}TST\text{-}TOT}$
240	3.05×10^{-10}	1.46×10^{-8}	9.97×10^{-19}	1.21×10^{-14}	1.49×10^{-8}
250	1.76×10^{-9}	4.74×10^{-8}	5.97×10^{-18}	6.97×10^{-14}	4.91×10^{-8}
260	9.01×10^{-9}	1.46×10^{-7}	3.30×10^{-17}	3.61×10^{-13}	1.55×10^{-7}
273	6.45×10^{-8}	5.92×10^{-7}	2.76×10^{-16}	2.65×10^{-12}	6.56×10^{-7}
280	1.74×10^{-7}	1.22×10^{-6}	8.39×10^{-16}	7.30×10^{-12}	1.40×10^{-6}
290	6.70×10^{-7}	3.33×10^{-6}	3.93×10^{-15}	2.91×10^{-11}	4.00×10^{-6}
298	1.86×10^{-6}	7.26×10^{-6}	1.32×10^{-14}	8.36×10^{-11}	9.12×10^{-6}
300	2.38×10^{-6}	8.80×10^{-6}	1.77×10^{-14}	1.08×10^{-10}	1.12×10^{-5}
310	7.90×10^{-6}	2.25×10^{-5}	7.70×10^{-14}	3.78×10^{-10}	3.04×10^{-5}
320	2.45×10^{-5}	5.60×10^{-5}	3.23×10^{-13}	1.25×10^{-9}	8.05×10^{-5}
330	7.17×10^{-5}	1.35×10^{-4}	1.31×10^{-12}	3.91×10^{-9}	2.07×10^{-4}
340	1.98×10^{-4}	3.19×10^{-4}	5.11×10^{-12}	1.17×10^{-8}	5.17×10^{-4}

T/K	*trans*-R8	*trans*-R8b	*trans*-R8c	*trans*-R8d	$k_{MC\text{-}TST\text{-}TOT}$
240	3.41×10^{-9}	3.73×10^{-8}	6.15×10^{-19}	4.87×10^{-15}	4.07×10^{-8}
250	1.82×10^{-8}	1.24×10^{-7}	3.58×10^{-18}	2.93×10^{-14}	1.42×10^{-7}
260	8.62×10^{-8}	3.90×10^{-7}	1.92×10^{-17}	1.57×10^{-13}	4.76×10^{-7}
273	5.60×10^{-7}	1.61×10^{-6}	1.56×10^{-16}	1.21×10^{-12}	2.17×10^{-6}
280	1.44×10^{-6}	3.34×10^{-6}	4.66×10^{-16}	3.40×10^{-12}	4.78×10^{-6}
290	5.16×10^{-6}	9.17×10^{-6}	2.14×10^{-15}	1.39×10^{-11}	1.43×10^{-5}
298	1.36×10^{-5}	2.00×10^{-5}	7.07×10^{-15}	4.10×10^{-11}	3.36×10^{-5}
300	1.71×10^{-5}	2.43×10^{-5}	9.48×10^{-15}	5.33×10^{-11}	4.14×10^{-5}
310	5.32×10^{-5}	6.21×10^{-5}	4.07×10^{-14}	1.91×10^{-10}	1.15×10^{-4}
320	1.55×10^{-4}	1.54×10^{-4}	1.70×10^{-13}	6.46×10^{-10}	3.09×10^{-4}
330	4.27×10^{-4}	3.70×10^{-4}	6.87×10^{-13}	2.07×10^{-09}	7.97×10^{-4}
340	1.11×10^{-3}	8.65×10^{-4}	2.69×10^{-12}	6.33×10^{-9}	1.98×10^{-3}

Table S10. Rate constants of the dissociation (R13), isomerization (R14), and H-abstraction (R15) of alkoxy radicals *cis*-RO and *trans*-RO computed at different temperatures (s^{-1} for R13 and R14, cm^3 $molecules^{-1}$ s^{-1} for R15).

T/*K*	*k*(R13)	*k*(R14)	*k*(R15)
240	6.06×10^{6}	3.72×10^{-2}	5.74×10^{-20}
250	1.09×10^{7}	6.35×10^{-2}	7.72×10^{-20}
260	1.89×10^{7}	1.09×10^{-1}	1.04×10^{-19}
273	3.64×10^{7}	1.88×10^{-1}	1.52×10^{-19}
280	5.06×10^{7}	3.25×10^{-1}	1.87×10^{-19}
290	7.88×10^{7}	5.64×10^{-1}	2.49×10^{-19}
298	1.10×10^{8}	8.78×10^{-1}	3.13×10^{-19}
300	1.19×10^{8}	9.81×10^{-1}	3.31×10^{-19}
310	1.76×10^{8}	1.71	4.37×10^{-19}
320	2.54×10^{8}	2.97	5.76×10^{-19}
330	3.59×10^{8}	5.16	7.54×10^{-19}
340	4.97×10^{8}	8.91	9.81×10^{-19}

Table S11. The atmospheric lifetimes of *cis*-BU and *trans*-BU in different regions.

		Guangzhou	Chongqing	Hongkong	Lanzhou	Housten
cis-BU	Min	2.48	1.24	1.06	3.54	0.34
	Ave	3.72	1.86	1.52	3.72	0.45
	Max	7.43	3.72	2.65	3.91	0.91
trans-BU	Min	1.58	0.79	0.68	2.26	0.22
	Ave	2.37	1.19	0.97	2.37	0.29
	Max	4.75	2.37	1.70	2.50	0.58

Table S12. AtChem 2 model settings. “new” and “base” represent the mechanism proposed in this study and the original MCM v3.3.1 mechanism, respectively. CBU indicates the consumption rate of BU, [CH_3COOH], $Y_{CH3COOH}$, and P(CH_3COOH) represent the concertation, yield, and average formation rate of CH_3COOH, respectively.

cis-BU	No.	[OH]	[BU]	[NO]	[NO_2]	C_{BU} (%)	[CH_3COOH] (ppb)	$Y_{CH3COOH}$ (%)	P(CH_3COOH) (ppb h^{-1})
new	1	8×10^5	1.23 $\times10^{11}$	4.92 $\times10^{10}$	4.18 $\times10^{11}$	86.3	3.82	46.2	0.33
	2	2×10^6				97.8	2.82	57.7	0.46
	3	6×10^6				100.0	3.22	64.3	0.51
	4	1×10^7				100.0	3.14	62.9	0.49
base	5	8×10^5	1.23 $\times10^{11}$	4.92 $\times10^{10}$	4.18 $\times10^{11}$	86.2	0.23	5.3	0.04
	6	2×10^6				97.8	0.16	3.2	0.03
	7	6×10^6				100.0	0.07	1.3	0.01
	8	1×10^7				100.0	0.04	4.1	0.01

cis-BU	No.	[OH]	[BU]	[NO]	[NO_2]	C_{BU} (%)	[CH_3COOH] (ppb)	$Y_{CH3COOH}$ (%)	P(CH_3COOH) (ppb h^{-1})
new	9	2×10^6	1.23 $\times10^{11}$	2.46 $\times10^{9}$	4.18 $\times10^{11}$	97.9%	2.81	57.4%	0.46
	10			2.46 $\times10^{10}$		97.9%	2.81	57.4%	0.46
	11			2.46 $\times10^{11}$		97.3%	2.92	60.0%	0.47
	12			5.00 $\times10^{11}$		96.6%	3.02	62.5%	0.49
base	13	2×10^6	1.23 $\times10^{11}$	2.46 $\times10^{9}$	4.18 $\times10^{11}$	98.0%	0.16	3.3%	0.03
	14			2.46 $\times10^{10}$		97.9%	0.16	3.2%	0.03
	15			2.46 $\times10^{11}$		97.9%	0.16	3.2%	0.03
	16			5.00 $\times10^{11}$		97.9%	0.16	3.2%	0.03

trans-BU	No.	[OH]	[BU]	[NO]	[NO_2]	C_{BU} (%)	[CH_3COOH] (ppb)	$Y_{CH3COOH}$ (%)	P(CH_3COOH) (ppb h^{-1})
new	17	8×10^5	1.23 $\times10^{11}$	4.92 $\times10^{10}$	4.18 $\times10^{11}$	93.2	1.93	41.5	0.31
	18	2×10^6				99.3	2.68	54.0	0.43
	19	6×10^6				100.0	3.12	62.3	0.48
	20	1×10^7				100.0	3.08	61.6	0.48
base	21	8×10^5	1.23	4.92	4.18	93.1	0.28	6.0	0.05

	22	2×10^{6}	$\times10^{11}$	$\times10^{10}$	$\times10^{11}$	99.3	0.19	3.8	0.03
	23	6×10^{6}				100.0	0.08	1.6	0.01
	24	1×10^{7}				100.0	0.05	1.0	0.01

trans-BU	No.	[OH]	[BU]	[NO]	[NO_2]	C_{BU} (%)	[CH_3COOH] (ppb)	$Y_{CH3COOH}$ (%)	P(CH_3COOH) (ppb h^{-1})
new	25	2×10^{6}	1.23×10^{11}	2.46×10^{9}	4.18×10^{11}	99.3%	2.65	53.4%	0.42
	26			2.46×10^{10}		99.3%	2.66	53.7%	0.43
	27			2.46×10^{11}		99.0%	2.80	56.5%	0.45
	28			5.00×10^{11}		98.6%	2.92	59.3%	0.47
base	29	2×10^{6}	1.23×10^{11}	2.46×10^{9}	4.18×10^{11}	99.3%	0.19	3.9%	0.03
	30			2.46×10^{10}		99.3%	0.19	3.8%	0.00
	31			2.46×10^{11}		99.3%	2.65	53.4%	0.42
	32			5.00×10^{11}		99.3%	2.66	53.7%	0.43

Table S13. The observed-based model inputs hourly concentrations of trace gases, meteorological parameters, and VOCs in the petrochemical industrial region.

Species/parameter	Mean	Median	Max
O_3 (ppb)	35.3	27.5	60.0
CO (ppb)	933.1	914.6	1040.7
NO (ppb)	3.6	2.2	10.4
NO_2 (ppb)	27.1	26.4	42.3
SO_2 (ppb)	50.3	34.9	108.5
Temperature (K)	300.6	300.6	303.9
Relative humidity (%)	40	40	40
Pressure (hPa)	1013.2	1013.2	1013.2
Alkanes (ppb)	22.5	19.7	37.4
Alkenes (ppb)	11.4	10.0	19.0
Aromatics (ppb)	5.6	4.9	9.3
Halocarbons (ppb)	9.4	8.2	15.6

Table S14. kinetic mechanism of the reaction of BU with OH

% 1.10D-11*EXP(487/TEMP) : CBUT2ENE + OH = BUT2OLO2 ;
% 3.22D-15*EXP(-968/TEMP) : CBUT2ENE + O3 = CH3CHO + CH3CHOOB ;
% 3.50D-13 : CBUT2ENE + NO3 = C42NO33O2 ;
% KDEC*0.18 : CH3CHOOB = CH3CHOO ;
% KDEC*0.57 : CH3CHOOB = CH3O2 + CO + OH ;
% KDEC*0.125 : CH3CHOOB = CH3O2 + HO2 ;
% KDEC*0.125 : CH3CHOOB = CH4 ;
% KRO2NO : C42NO33O2 + NO = C42NO33O + NO2 ;
% KROSEC*O2 : C42NO33O = BUTONENO3 + HO2 ;
% 4.00D+04 : C42NO33O = CH3CHO + CH3CHO + NO2 ;
% KRO2NO3 : C42NO33O2 + NO3 = C42NO33O + NO2 ;
% KRO2HO2*0.625 : C42NO33O2 + HO2 = C42NO33OOH ;
% 2.50D-13*0.6*RO2 : C42NO33O2 = C42NO33O ;
% 2.50D-13*0.2*RO2 : C42NO33O2 = BUTONENO3 ;
% 2.50D-13*0.2*RO2 : C42NO33O2 = BUT2OLNO3 ;
% J<41> : C42NO33OOH = C42NO33O + OH ;
% 7.15D-12 : C42NO33OOH + OH = BUTONENO3 + OH ;
% 1.2D-12 : BUTONENO3 + OH = BIACET + NO2 ;
% J<56>*1.6 : BUTONENO3 = MEKBO + NO2 ;
% 3.8D-13*EXP(780/TEMP)*(1/(1+498*EXP(-1160/TEMP))) : CH3O2 + HO2 = HCHO ;
% 4.7D-12*EXP(345/TEMP)*0.05 : CH3CHO + OH = HCOCH2O2 ;
% J<31> : GLYOX = CO + CO + H2 ;
% J<32> : GLYOX = CO + HCHO ;
% J<33> : GLYOX = CO + CO + HO2 + HO2 ;
% 3.1D-12*EXP(340/TEMP) : GLYOX + OH = HCOCO ;

% KNO3AL : GLYOX + NO3 = HCOCO + HNO3 ;
% KAPNO : HCOCO3 + NO = CO + HO2 + NO2 ;
% KFPAN : HCOCO3 + NO2 = CO + HO2 + NO3 ;
% KRO2NO3*1.74 : HCOCO3 + NO3 = CO + HO2 + NO2 ;
% KAPHO2*0.41 : HCOCO3 + HO2 = HCOCO3H ;
% KAPHO2*0.15 : HCOCO3 + HO2 = HCOCO2H + O3 ;
% 1.00D-11*0.7*RO2 : HCOCO3 = CO + HO2 ;
% 1.00D-11*0.3*RO2 : HCOCO3 = HCOCO2H ;
% 1.58D-11 : HCOCO3H + OH = HCOCO3 ;
% J<41> : HCOCO3H = CO + HO2 + OH ;
% J<15> : HCOCO3H = CO + HO2 + OH ;
% 1.23D-11 : HCOCO2H + OH = CO + HO2 ;
% 5.4D-12*EXP(135/TEMP) : HCHO + OH = CO + HO2 ;
% J<11> : HCHO = CO + HO2 + HO2 ;
% J<12> : HCHO = CO + H2 ;
% 5.5D-16 : HCHO + NO3 = CO + HNO3 + HO2 ;
% 4.7D-12*EXP(345/TEMP)*0.95 : CH3CHO + OH = CH3CO3 ;
% 1.4D-12*EXP(-1860/TEMP) : CH3CHO + NO3 = CH3CO3 + HNO3 ;
% 7.5D-12*EXP(290/TEMP) : CH3CO3 + NO = CH3O2 + NO2 ;
% KFPAN : CH3CO3 + NO2 = PAN ;
% KBPAN : PAN = CH3CO3 + NO2 ;
% 4.0D-12 : CH3CO3 + NO3 = CH3O2 + NO2 ;
% KAPHO2*0.41 : CH3CO3 + HO2 = CH3CO3H ;
% KAPHO2*0.15 : CH3CO3 + HO2 = CH3CO2H + O3 ;
% 1.00D-11*0.7*RO2 : CH3CO3 = CH3O2 ;
% 1.00D-11*0.3*RO2 : CH3CO3 = CH3CO2H ;
% 3D-14 : OH + PAN = CO + HCHO + NO2 ;

% J<41> : CH3CO3H = CH3O2 + OH ;
% 3.70D-12 : CH3CO3H + OH = CH3CO3 ;
% J<13> : CH3CHO = CH3O2 + CO + HO2 ;
% KRO2NO : HCOCH2O2 + NO = HCOCH2O + NO2 ;
% KDEC : HCOCH2O = CO + HCHO + HO2 ;
% KRO2NO3 : HCOCH2O2 + NO3 = HCOCH2O + NO2 ;
% KRO2HO2*0.387 : HCOCH2O2 + HO2 = HCOCH2OOH ;
% 2.00D-12*0.6*RO2 : HCOCH2O2 = HCOCH2O ;
% 2.00D-12*0.2*RO2 : HCOCH2O2 = GLYOX ;
% 2.00D-12*0.2*RO2 : HCOCH2O2 = HOCH2CHO ;
% J<41> : HCOCH2OOH = HCOCH2O + OH ;
% J<15> : HCOCH2OOH = CO + HCHO + HO2 + OH ;
% 1.90D-12*EXP(190/TEMP) : HCOCH2OOH + OH = HCOCH2O2 ;
% 2.91D-11 : HCOCH2OOH + OH = GLYOX + OH ;
% KDEC : MEKBO = CH3CHO + CH3CO3 ;
% 2.85D-12*EXP(-345/TEMP) : CH3OH + OH = HCHO + HO2 ;
% KRO2NO*0.959 : BUT2OLO2 + NO = BUT2OLAO + NO2 ;
% KRO2NO*0.041 : BUT2OLO2 + NO = BUT2OLNO3 ;
% 1.97D+13*EXP(-3602.43/TEMP) : BUT2OLAO = CH3CHO + CH3CHOH ;
% 1.0D-11*O2 : CH3CHOH = CH3CHONEW + HO2 ;
% 4.7D-12*EXP(345/TEMP)*0.05 : CH3CHONEW + OH = HCOCH2O2 ;
% 4.7D-12*EXP(345/TEMP)*0.95 : CH3CHONEW + OH = CH3CO3 ;
% 1.4D-12*EXP(-1860/TEMP) : CH3CHONEW + NO3 = CH3CO3 + HNO3 ;
% J<13> : CH3CHONEW = CH3O2 + CO + HO2 ;
% 4.8D-11*O2 : CH3CHOH = CH3CHOHRO2 ;
% KRO2NO : CH3CHOHRO2 + NO = CH3CHOHRO ;
% 1.67D+2 : CH3CHOHRO = CH3COOHNEW + HO2;

% 8.00D-13 : CH3COOHNEW + OH = CH3O2 ;
% KRO2NO3 : BUT2OLO2 + NO3 = BUT2OLAO + NO2 ;
% KRO2HO2*0.625 : BUT2OLO2 + HO2 = BUT2OLOOH ;
% 8.80D-13*0.6*RO2 : BUT2OLO2 = BUT2OLAO ;
% 8.80D-13*0.2*RO2 : BUT2OLO2 = BUT2OLO ;
% 8.80D-13*0.2*RO2 : BUT2OLO2 = BUT2OLOH ;
% 1.79D-12 : BUT2OLNO3 + OH = BUT2OLO + NO2 ;
% 2.89D-11 : BUT2OLOOH + OH = BUT2OLO + OH ;
% J<41> : BUT2OLOOH = BUT2OLAO + OH ;
% 1.90D-12*EXP(190/TEMP) : BUT2OLOOH + OH = BUT2OLO2 ;
% 5.86D-12 : BUT2OLO + OH = BIACET + HO2 ;
% J<22> : BUT2OLO = CH3CHO + CH3CO3 + HO2 ;
% 1.73D-11 : BUT2OLOH + OH = BUT2OLO + HO2 ;
% 8.00D-13 : CH3CO2H + OH = CH3O2 ;
% J<34> : CO23C3CHO = CH3CO3 + CO + CO + HO2 ;
% J<35> : CO23C3CHO = CH3CO3 + HCOCO ;
% J<34> : HCOCO2H = CO + HO2 + HO2 ;
% 1.12D-12 : OH + PHAN = CO + HCHO + NO2 ;
% KAPHO2*0.44 : CH3CO3 + HO2 = CH3O2 + OH ;
% KAPHO2*0.44 : HCOCO3 + HO2 = CO + HO2 + OH ;
% KAPHO2*0.44 : HO2 + HOCH2CO3 = HCHO + HO2 + OH ;
% 7.00D11*EXP(-3160/TEMP) : HCOCO = CO + CO + HO2 ;
% 5.00D-12*O2 : HCOCO = CO + CO + HO2 ;
% 5.00D-12*O2*3.2*EXP(-550/TEMP) : HCOCO = HCOCO3 ;
% 5.00D-12*O2*3.2*(1-EXP(-550/TEMP)) : HCOCO = CO + OH ;
% 1.85D-12*EXP(-1690/TEMP) : CH4 + OH = CH3O2 ;
% 2.3D-12*EXP(360/TEMP)*0.999 : CH3O2 + NO = CH3O + NO2 ;

% 2.3D-12*EXP(360/TEMP)*0.001 : CH3O2 + NO = CH3NO3 ;
% 7.2D-14*EXP(-1080/TEMP)*O2 : CH3O = HCHO + HO2 ;
% KMT13 : CH3O2 + NO2 = CH3O2NO2 ;
% KMT14 : CH3O2NO2 = CH3O2 + NO2 ;
% 1.2D-12 : CH3O2 + NO3 = CH3O + NO2 ;
% 3.8D-13*EXP(780/TEMP)*(1-1/(1+498*EXP(-1160/TEMP))) : CH3O2 + HO2 = CH3OOH ;
% 2*KCH3O2*RO2*7.18*EXP(-885/TEMP) : CH3O2 = CH3O ;
% 2*KCH3O2*RO2*0.5*(1-7.18*EXP(-885/TEMP)) : CH3O2 = HCHO ;
% 2*KCH3O2*RO2*0.5*(1-7.18*EXP(-885/TEMP)) : CH3O2 = CH3OH ;
% 4.0D-13*EXP(-845/TEMP) : CH3NO3 + OH = HCHO + NO2 ;
% J<51> : CH3NO3 = CH3O + NO2 ;
% 5.3D-12*EXP(190/TEMP)*0.6 : CH3OOH + OH = CH3O2 ;
% 5.3D-12*EXP(190/TEMP)*0.4 : CH3OOH + OH = HCHO + OH ;
% J<41> : CH3OOH = CH3O + OH ;
% J<35> : BIACET = CH3CO3 + CH3CO3 ;
% 1.40D-18*TEMP@(2)*EXP(194/TEMP) : BIACET + OH = BIACETO2 ;
% KRO2NO : BIACETO2 + NO = BIACETO + NO2 ;
% KDEC : BIACETO = CH3CO3 + CO + HCHO ;
% KRO2NO3 : BIACETO2 + NO3 = BIACETO + NO2 ;
% KRO2HO2*0.625 : BIACETO2 + HO2 = BIACETOOH ;
% 2.00D-12*0.6*RO2 : BIACETO2 = BIACETO ;
% 2.00D-12*0.2*RO2 : BIACETO2 = BIACETOH ;
% 2.00D-12*0.2*RO2 : BIACETO2 = CO23C3CHO ;
% 5.99D-12 : BIACETOOH + OH = CO23C3CHO + OH ;
% 1.90D-12*EXP(190/TEMP) : BIACETOOH + OH = BIACETO2 ;
% J<41> : BIACETOOH = BIACETO + OH ;

% J<35> : BIACETOOH = BIACETO + OH ;
% 2.69D-12 : BIACETOH + OH = CO23C3CHO + HO2 ;
% J<35> : BIACETOH = CH3CO3 + HOCH2CO3 ;
% 1.23D-11 : CO23C3CHO + OH = CH3CO3 + CO + CO ;
% KNO3AL*4.0 : CO23C3CHO + NO3 = CH3CO3 + CO + CO + HNO3 ;
% 6.6D-12*EXP(-1240/TEMP) : CH4 + CL = CH3O2 ;
% 1.00D-11*0.800 : HOCH2CHO + OH = HOCH2CO3 ;
% 1.00D-11*0.200 : HOCH2CHO + OH = GLYOX + HO2 ;
% J<15> : HOCH2CHO = CO + HCHO + HO2 + HO2 ;
% KNO3AL : HOCH2CHO + NO3 = HNO3 + HOCH2CO3 ;
% KFPAN : HOCH2CO3 + NO2 = PHAN ;
% KBPAN : PHAN = HOCH2CO3 + NO2 ;
% KAPNO : HOCH2CO3 + NO = HCHO + HO2 + NO2 ;
% KRO2NO3*1.74 : HOCH2CO3 + NO3 = HCHO + HO2 + NO2 ;
% KAPHO2*0.41 : HO2 + HOCH2CO3 = HOCH2CO3H ;
% KAPHO2*0.15 : HO2 + HOCH2CO3 = HOCH2CO2H + O3 ;
% 1.00D-11*0.7*RO2 : HOCH2CO3 = HCHO + HO2 ;
% 1.00D-11*0.3*RO2 : HOCH2CO3 = HOCH2CO2H ;
% 2.73D-12 : HOCH2CO2H + OH = HCHO + HO2 ;
% J<41> : HOCH2CO3H = HCHO + HO2 + OH ;
% 6.19D-12 : HOCH2CO3H + OH = HOCH2CO3 ;
% 1.00D-14 : CH3CHOO + NO = CH3CHO + NO2 ;
% 1.00D-15 : CH3CHOO + NO2 = CH3CHO + NO3 ;
% 7.00D-14 : CH3CHOO + SO2 = CH3CHO + SO3 ;
% 1.00D-17*H2O : CH3CHOO = CH3CO2H ;
% 6.00D-18*H2O : CH3CHOO = CH3CHO + H2O2 ;
% 1.20D-15 : CH3CHOO + CO = CH3CHO ;

References

Chen, L., Huang, Y., Xue, Y., Jia, Z., and Wang, W.: OH-initiated atmospheric degradation of hydroxyalkyl hydroperoxides: mechanism, kinetics, and structure–activity relationship, Atmos. Chem. Phys., 22, 3693-3711, https://doi.org/10.5194/acp-22-3693-2022, 2022.

Jenkin, M. E., Saunders, S. M., and Pilling, M. J.: The tropospheric degradation of volatile organic compounds: a protocol for mechanism development, Atmos. Environ., 31, 81-104, https://doi.org/10.1016/S1352-2310(96)00105-7, 1997.

Møller, K. H., Otkjær, R. V., Hyttinen, N., Kurtén, T., and Kjaergaard, H. G.: Cost-Effective Implementation of Multiconformer Transition State Theory for Peroxy Radical Hydrogen Shift Reactions, J. Phys. Chem. A, 120, 10072-10087, https://doi.org/10.1021/acs.jpca.6b09370, 2016.

Saunders, S. M., Jenkin, M. E., Derwent, R. G., and Pilling, M. J.: Protocol for the development of the Master Chemical Mechanism, MCM v3 (Part A): tropospheric degradation of non-aromatic volatile organic compounds, Atmos. Chem. Phys., 3, 161-180, https://doi.org/10.5194/acp-3-161-2003, 2003.

Sommariva, R., Cox, S., Martin, C., Borońska, K., Young, J., Jimack, P. K., Pilling, M. J., Matthaios, V. N., Nelson, B. S., Newland, M. J., Panagi, M., Bloss, W. J., Monks, P. S., and Rickard, A. R.: AtChem (version 1), an open-source box model for the Master Chemical Mechanism, Geosci. Model Dev., 13, 169-183, https://doi.org/10.5194/gmd-13-169-2020, 2020.

Yang, J., Zeren, Y., Guo, H., Wang, Y., Lyu, X., Zhou, B., Gao, H., Yao, D., Wang, Z., Zhao, S., Li, J., and Zhang, G.: Wintertime ozone surges: The critical role of alkene ozonolysis, Environ. Sci. Ecotechnol., 22, 100477, https://doi.org/10.1016/j.ese.2024.100477, 2024.

Yang, Y., Guo, W., Sun, J., Chen, Q., Meng, X., Wang, L., Tao, H., and Yang, L.: Characteristics of volatile organic compounds and secondary organic aerosol pollution in different functional areas of petrochemical industrial cities in Northwest China, Sci. Total Environ., 858, 159903, https://doi.org/10.1016/j.scitotenv.2022.159903, 2023.